ELSEVIER

Journal of Structural Geology 27 (2005) 2135–2149

JOURNAL OF STRUCTURAL GEOLOGY

www.elsevier.com/locate/jsg

Influence of object concentration on finite strain and effective viscosity contrast: insights from naturally deformed packstones

Stefano Vitale*, Stefano Mazzoli

Dipartimento di Scienze della Terra, Università degli studi di Napoli 'Federico II', Largo San Marcellino 10, 80138 Napoli, Italy

Received 12 May 2005; received in revised form 6 July 2005; accepted 2 August 2005
Available online 12 September 2005

Abstract

Deformed conglomerates and ooidal/oncoidal packstones are commonly used to evaluate finite strain in deformed sedimentary successions. In order to obtain a correct estimate of finite strain, it is necessary to consider not only the different behaviour of matrix and objects, but also object concentration. The analysis of two-component rocks characterised by high values of packing commonly results in a substantial underestimate of bulk strain and of viscosity contrast between objects and matrix. In this study, the effects of the volumetric fraction of competent inclusions on both object and bulk measured finite strain, as well as on apparent viscosity contrast, have been investigated in naturally deformed packstones characterised by variable object concentration on the scale of the hand specimen (and hence for homogenous viscosity contrast). Object finite strain has been obtained by Rf/ϕ analysis, whereas the Fry method provides a measure of whole-rock strain that is also a function of inclusion concentration. Therefore, the finite strain measured by the Fry method is better termed *effective bulk strain*. In order to investigate the role of object concentration, this parameter has been plotted against object and effective bulk strain, and also against viscosity contrast. These diagrams show that: (i) for high values of packing, measured object and effective bulk strain show values that are significantly lower with respect to the calculated maximum value (that would result in the ideal case of no particle interaction and represents therefore the *real bulk strain* of the samples); (ii) the viscosity contrast shows lower values with respect to the calculated maximum one (that is equal for the three principal sections of the finite strain ellipsoid), and as packing reaches the maximum value, the viscosity contrast approaches a unit value. Empirical equations have also been found that link object concentration with both object and effective bulk finite strain.

Keywords: Strain analysis; Object strain; Bulk strain; Very low-grade limestones; Italy

1. Introduction

The easiest and most used methods for evaluating finite strain in deformed rocks involve the study of strain markers such as clasts in deformed conglomerates and fossils or ooids in grainstones and packstones (Cloos, 1947; Ramsay and Huber, 1983). However, the simple assumption that objects such as pebbles or ooids behave as passive markers during ductile deformation—and therefore are representative of bulk finite strain—is usually not valid due to the occurrence of viscosity contrasts between objects and matrix (Gay, 1968a).

In most rocks consisting of two components (objects and matrix), the finite strain measured from the objects represents a substantial underestimate of bulk finite strain because the objects are generally more competent than the matrix. Well-established techniques of finite strain analysis (Ramsay and Huber, 1983) are nowadays implemented by computer software, allowing a fast evaluation of object and bulk finite strain by image analysis. Furthermore, several papers provide a complete theory of deformation for objects embedded in a matrix characterised by different rheological behaviour (Gay, 1968a,b, 1976; Bilby et al., 1975; Treagus and Treagus, 2001, 2002). Nevertheless, all the methods and calculations developed for the evaluation of finite strain and viscosity contrast between objects and matrix assume idealised settings whereby each object is not influenced by surrounding ones. Although it is well known that naturally

* Corresponding author. Present address: Department of Geology, University of New Brunswick, Fredericton, NB, Canada E3B 5A3. Tel.: +39 081258162; fax: +39 0815525611.
E-mail address: stvitale@unina.it (S. Vitale).

0191-8141/$ - see front matter © 2005 Elsevier Ltd. All rights reserved.
doi:10.1016/j.jsg.2005.08.001

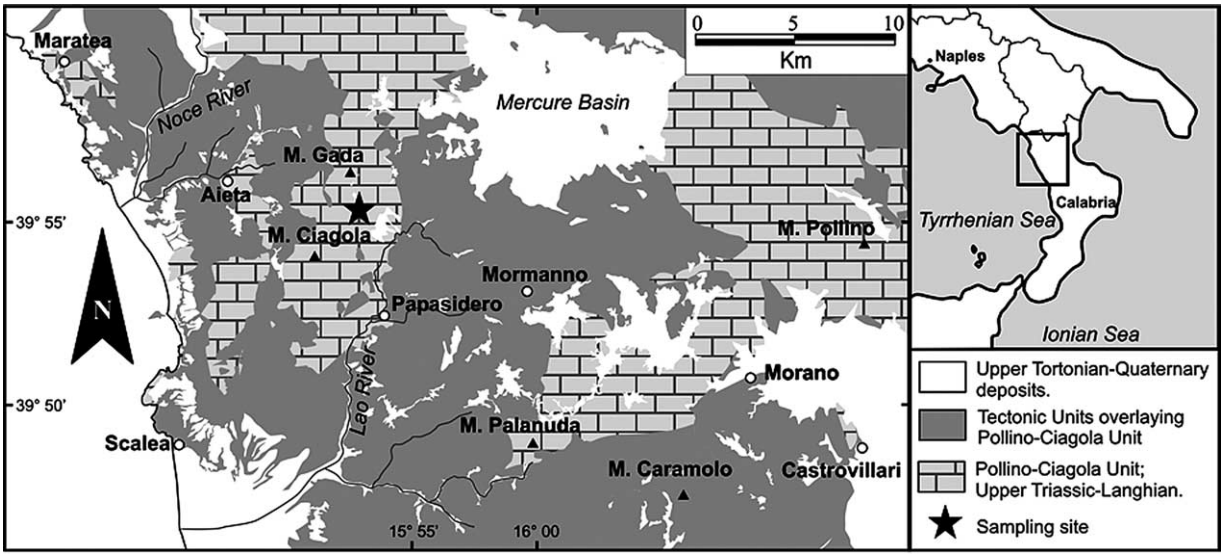

Fig. 1. Sketch map of northern Calabria, showing the sampled (Pollino-Ciagola) carbonate unit and tectonically overlying nappes (undifferentiated).

deformed rocks depart from this ideal condition, especially for high values of packing—and hence interaction among objects (Gay, 1968a)—to our knowledge a quantitative analysis of the role of object concentration in deformation has never been carried out in naturally deformed rocks. Such an analysis requires rock samples characterised by variable object concentration in a material maintaining a constant viscosity contrast, a condition not easy to meet. The availability, in our study area, of two-component rocks characterised by variable object concentration at the scale of the single hand specimen provides a rare opportunity to carry out an analysis of this type. The relationships between object concentration, finite strain and viscosity contrast are fully established for the analysed samples. The aim is to gain new insights into the general deformation behaviour of two-component rocks, including those commonly characterised by roughly constant object concentration, for which an analysis of the type carried out here is not possible. Our results provide a better constraint on the implications and limitations of finite strain analysis in rocks consisting of objects and matrix, enhancing the use of finite strain data from these rather common and intensely studied rock types.

2. Previous studies

Gay (1968a,b) investigated the role of viscosity contrast in rock deformation. This author, considering objects and matrix as highly viscous fluids, provided a linear equation linking bulk strain ratio (R_s) with object strain ratio (R_o) as a function of the viscosity contrast (r_{om}) between objects and matrix. However, Bilby et al. (1975) later rewrote the equation in a non-linear form:

$$\ln(R_s) = \ln(R_o) + (r_{om} - 1)\left(\frac{R_o - 1}{R_o + 1}\right) \quad (1)$$

Both equations can be applied only for objects that are not influenced by surrounding ones, i.e. when object concentration is very low. On the other hand, in naturally deformed rocks such as conglomerates, the latter constraint is routinely inappropriate because object concentration reaches high values. Gay (1968a) noted that the effective viscosity contrast decreases rapidly with increasing object concentration and proposed a theoretical equation relating: (i) the viscosity contrast between individual objects and the rock (r_{or}), and (ii) the viscosity contrast between objects and matrix (r_{om}), by the volume concentration of objects (C_v) and an interaction factor (ψ). The equation is expressed as:

$$r_{or} = \frac{r_{om}}{\left(1 + 5\psi C_v \frac{r_{om}-1}{2r_{om}+3}\right)}. \quad (2)$$

However, analogue modelling carried out by the same author suggested a different behaviour from the theoretical one, as the effective viscosity ratio between objects and rock decreases more rapidly than predicted.

Lisle (1979), analysing the finite strain of deformed conglomerates, suggested that for high values of packing, as in clast-supported conglomerates, the role of the matrix is negligible and therefore clast strain corresponds to bulk strain.

Finally, Mandal et al. (2003) analysed a two-phase mixture and provided a theoretical equation linking the ratio of object and bulk strain rate ($\dot{e}_o/\dot{e}_s$) with the ratio of object centre distance (b) and object radius (a) for different values of viscosity contrast. They pointed out that the curve that represents the velocity ratio $\dot{e}_o/\dot{e}_s$ (Mandal et al., 2003, their fig. 2) does not change for low object concentrations, whereas there is a rapid drop to unit as the a/b ratio approaches the minimum value (that is maximum packing). Furthermore, when the objects are more competent than the matrix, the object strain rate is lower than that for the bulk

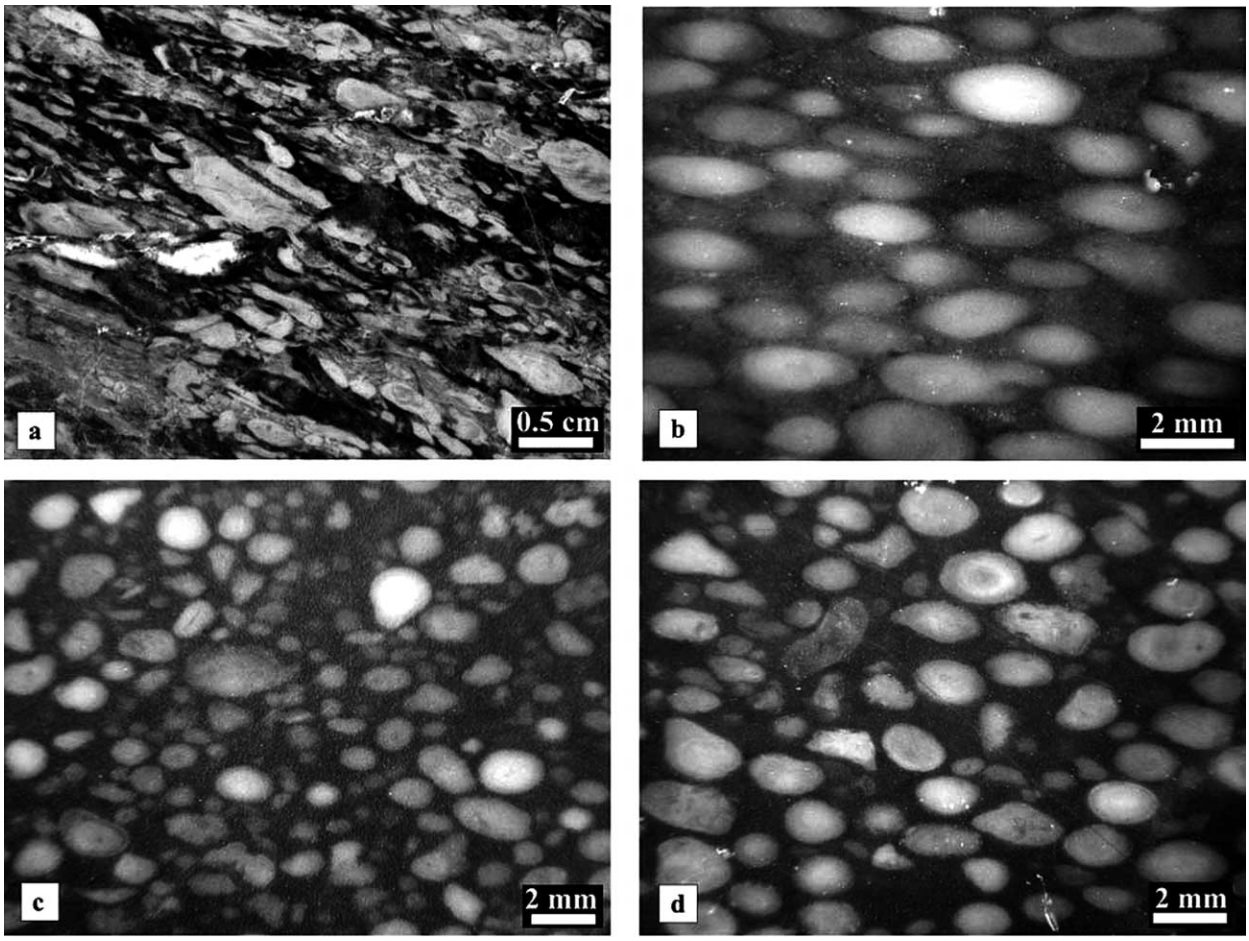

Fig. 2. Details of polished slabs cut parallel to the *XZ* principal section of the finite strain ellipsoid. (a) Sample 1: Jurassic oncoidal packstones. (b)–(d) Samples 2–4, respectively: Jurassic ooidal packstones.

rock and both approach the same value for high object concentration.

These studies suggest that the viscosity contrast between objects and rock and the ratio of object and rock strain rate are closely related to object concentration, especially for high values of packing. Hence, for the latter condition, the measured viscosity contrast represents an underestimate of the real value (i.e. that characterising the system in the ideal case of no particle interaction; Lisle et al, 1983). For these reasons, the measured viscosity contrast is better termed 'effective viscosity contrast' (Gay, 1968a).

3. Strain analysis

3.1. Materials

The studied samples are Mesozoic packstones from the sedimentary succession of the Pollino-Ciagola Unit (Vitale and Iannace, 2004) of northern Calabria (southern Italy; Fig. 1). This unit is characterised by a Norian–Langhian pelite–carbonate succession recording an evolution from carbonate platform to margin-slope and finally to foredeep environments. This unit has been affected by ductile deformation localised in narrow shear zones at several stratigraphic levels under very low-grade conditions (Iannace and Vitale, 2004; Vitale and Iannace, 2004). The deformed samples come from a Jurassic carbonate margin succession characterised by an alternation of oncoidal and ooidal packstones, wackestones and calcareous conglomerates. In order to evaluate the influence of packing on strain, selected samples characterised by variable object concentration were collected.

Four samples have been studied (Fig. 2): the first is an oncoidal packstone (sample 1), the others are ooidal packstones (samples 2–4). The samples were cut parallel to *XZ*, *YZ* and *XY* sections of the finite strain ellipsoid (mutually orthogonal sections defined by the foliation and stretching lineation; Ramsay and Huber, 1983) with an estimated maximum angle error of 5°. Each sample was divided into arbitrary sectors, each having a constant object concentration. For sample 1, a full 3D strain analysis was performed in order to investigate viscosity contrast and deformation behaviour on the three principal finite strain ellipsoid sections; for the others, only *XZ* principal sections were analysed.

Table 1
Results of the strain analysis for sample 1 (*XZ*, *YZ* and *XY* sections) and for samples 2–4 (*XZ* section). The viscosity contrast between objects and matrix (r_{om}) was calculated by Eq. (3)

Sample 1

XZ					*YZ*					*XY*				
C_o ($\pm$0.05)	R_s ($\pm$0.10)	R_o ($\pm$0.05)	r_{om}	Δr_{om}	C_o ($\pm$0.05)	R_s ($\pm$0.10)	R_o ($\pm$0.05)	r_{om}	Δr_{om}	C_o ($\pm$0.05)	R_s ($\pm$0.10)	R_o ($\pm$0.05)	r_{om}	Δr_{om}
0.39	4.45	3.29	1.57	0.06	0.41	3.45	2.64	1.59	0.10	0.44	2.81	2.24	1.59	0.14
0.45	4.08	3.08	1.55	0.07	0.62	2.43	2.12	1.38	0.17	0.53	2.67	2.14	1.61	0.15
0.50	3.97	3.00	1.56	0.08	0.65	2.03	1.95	1.12	0.23	0.63	2.26	1.93	1.50	0.20
0.52	4.26	3.10	1.62	0.07	0.67	1.95	1.95	1.00	0.24	0.64	2.02	1.80	1.40	0.25
0.64	2.72	2.32	1.40	0.14	0.66	1.89	1.88	1.02	0.26	0.64	2.17	1.91	1.41	0.22
0.65	2.54	2.35	1.19	0.15	0.66	2.00	1.90	1.16	0.24	0.65	1.96	1.76	1.39	0.27
0.66	2.24	2.19	1.06	0.18	0.66	1.64	1.52	1.4	0.4					
0.66	2.66	2.42	1.23	0.14										
$(C_o)_{max}=0.66$														

Sample 2					Sample 3					Sample 4				
XZ					*XZ*					*XZ*				
C_o ($\pm$0.05)	R_s ($\pm$0.10)	R_o ($\pm$0.05)	r_{om}	Δr_{om}	C_o ($\pm$0.05)	R_s ($\pm$0.10)	R_o ($\pm$0.05)	r_{om}	Δr_{om}	C_o ($\pm$0.05)	R_s ($\pm$0.10)	R_o ($\pm$0.05)	r_{om}	Δr_{om}
0.53	2.22	2.00	1.31	0.20	0.54	2.03	1.51	2.43	0.29	0.43	1.97	1.75	1.43	0.27
0.52	2.30	2.07	1.30	0.18	0.53	1.97	1.45	2.66	0.31	0.50	1.79	1.67	1.30	0.33
0.49	2.60	2.21	1.43	0.15	0.54	1.61	1.41	1.7	0.5	0.50	1.73	1.65	1.20	0.35
0.34	3.10	2.48	1.52	0.11	0.29	2.54	1.54	3.35	0.20	0.41	2.02	1.70	1.66	0.27
0.35	3.17	2.52	1.53	0.11	0.30	2.43	1.48	3.56	0.25					
0.53	1.43	1.38	1.2	0.6										
0.39	2.31	1.46	3.45	0.27										
0.50	1.50	1.41	1.4	0.6										
$(C_o)_{max}=0.53$					$(C_o)_{max}=0.55$					$(C_o)_{max}=0.50$				

3.2. Methods

The most commonly reported methods for evaluating object finite strain are the harmonic mean of the object aspect ratios (Lisle, 1979) and the Rf/ϕ method (Ramsay, 1967; Dunnet, 1969; Lisle, 1985) by the eyeballing-in best-fit technique (Ramsay and Huber, 1983). The use of one of these methods alone may not furnish an accurate evaluation of finite strain because (i) the harmonic mean is always an overestimate of real strain (Lisle, 1979) and (ii) if the Rf/ϕ distribution is not symmetric the method does not provide a correct result. In this study, we used both methods in order to compare results and obtain an estimate of their accuracy.

Likewise, the easiest and most used technique for the evaluation of bulk finite strain is the Fry analysis (Fry, 1979) and the normalised centre-to-centre technique (Erslev, 1988).

Strain analysis was performed on images of polished slabs parallel to sections of the finite strain ellipsoid. The images were analysed by the ImageJ software (free software, http://rbs.info.nih.gov/ij/) in order to determine the major and minor axes of the best-fit ellipse, the angle that the major axis makes with a reference direction, and finally the object area fraction. Where object size was fairly homogeneous the Fry method was used (performed by means of the GeoFryPlots software; author: Rod Holcombe, web site http://www.earth.uq.edu.au), whereas for variable object size the normalised centre-to-centre method was applied.

In order to estimate the viscosity contrast between objects and matrix (r_{om}) we used the equation (Bilby et al., 1975; Gay, 1976):

$$r_{om} = \frac{R_o + 1}{R_o - 1} \ln\left(\frac{R_s}{R_o}\right) + 1 \tag{3}$$

where R_s is the bulk finite strain and R_o is the object finite strain.

3.3. Results

The results of the strain analysis are summarised in Table 1, whereas Fig. 3 shows an example of the analysis carried out using both the Rf/ϕ and Fry methods.

In order to estimate the variation of finite strain (for both objects and rock) and of the viscosity contrast between objects and matrix (r_{om}) related to the object area fraction (C_o), plots of $R_o - R_s$ versus C_o (Fig. 4) and r_{om} versus C_o were generated (Fig. 5). We chose for object strain error (ΔR_o) a maximum value of 0.05, for bulk strain error (ΔR_s) a value of 0.10 and finally for the concentration error (ΔC_o) a value of 0.05. All of the latter are related to instrumental precision.

To evaluate the viscosity contrast error we used the propagation law for maximal errors:

$$\Delta f(x) = \sum_i \left(\left| \frac{\partial f(x)}{\partial x_i} \right| \Delta xi \right) \tag{4}$$

where $f(x_i) = r_{om}(R_o, R_s)$ is obtained from Eq. (3).

4. Discussion

Finite strain appears to be non-homogenous on the scale of the sample, higher values of strain (both R_o and R_s) characterising those parts of the samples having lower object area fraction (C_o), whereas minimum values of R_o and R_s are reached when the object area fraction corresponds to a high value of packing (Fig. 4). Fig. 4a also shows that the minimum values of R_o and R_s are different for the three finite strain ellipsoid sections.

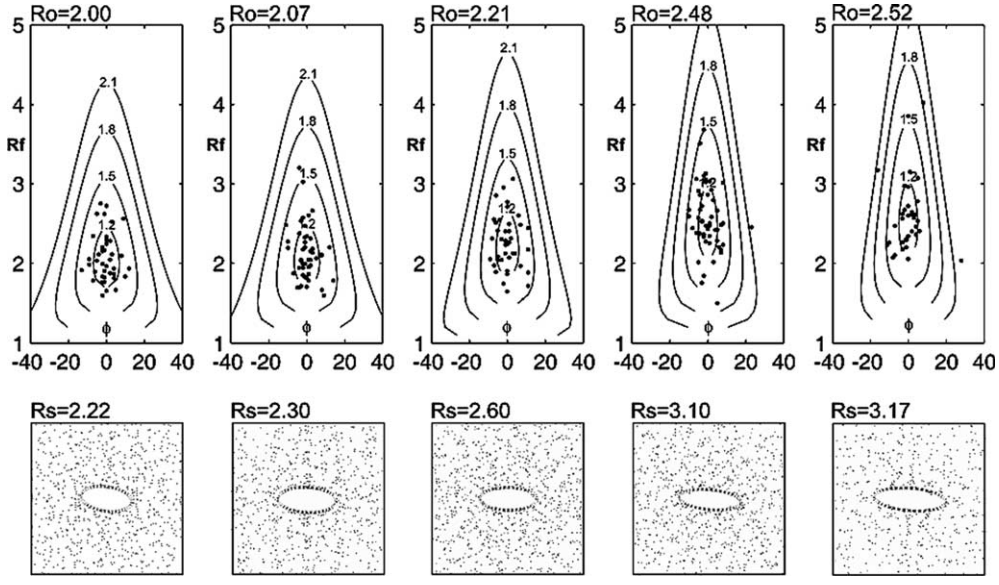

Fig. 3. Examples of Rf/ϕ and Fry diagrams (*XZ* principal section of sample 2). Solid lines indicate original aspect ratios.

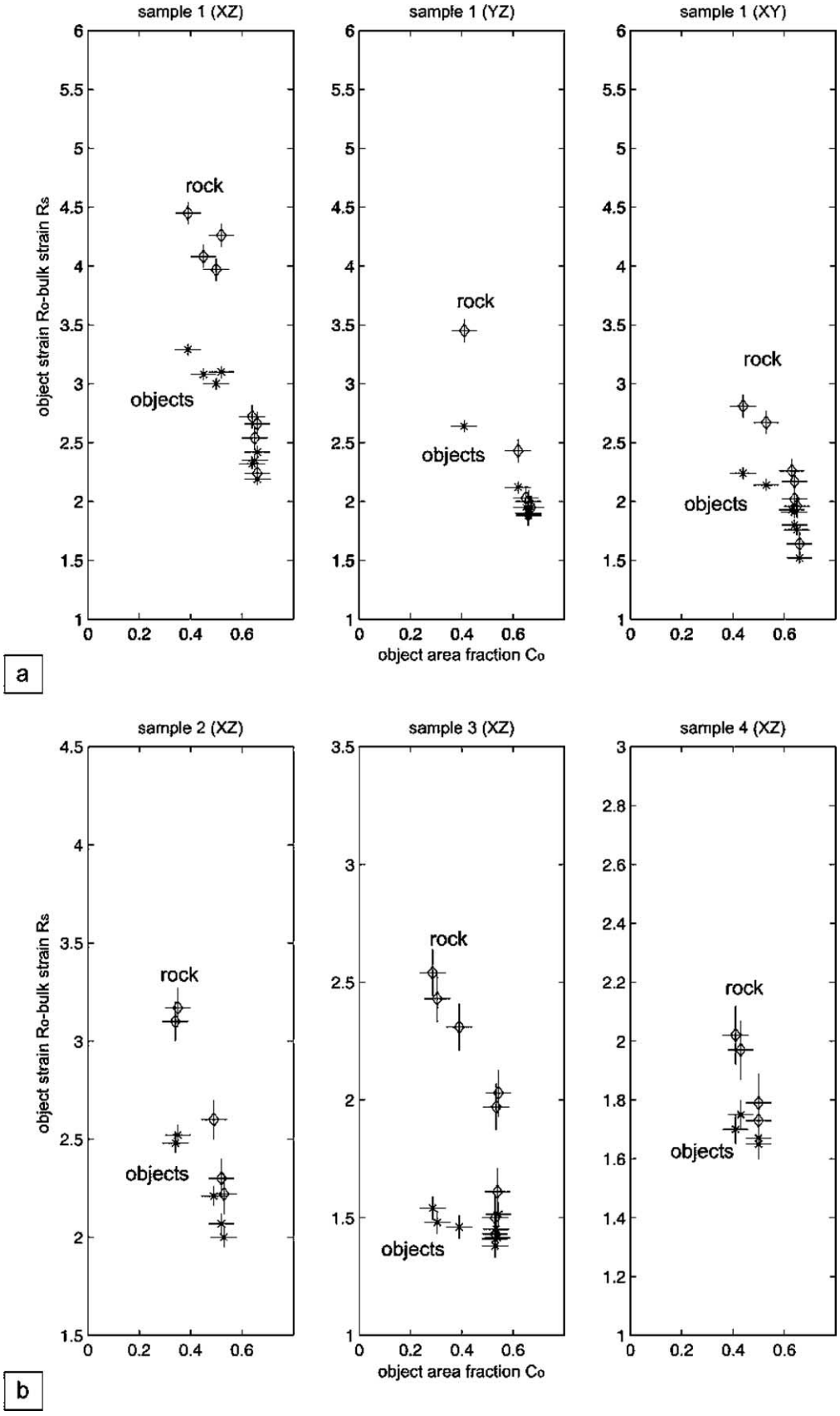

Fig. 4. Plots of measured object and bulk strain versus object area fraction (stars represent R_o–C_o couples, diamonds represent R_s–C_o couples). (a) Sample 1 (*XZ*, *YZ* and *XY* principal sections). (b) Samples 2–4 (*XZ* principal sections).

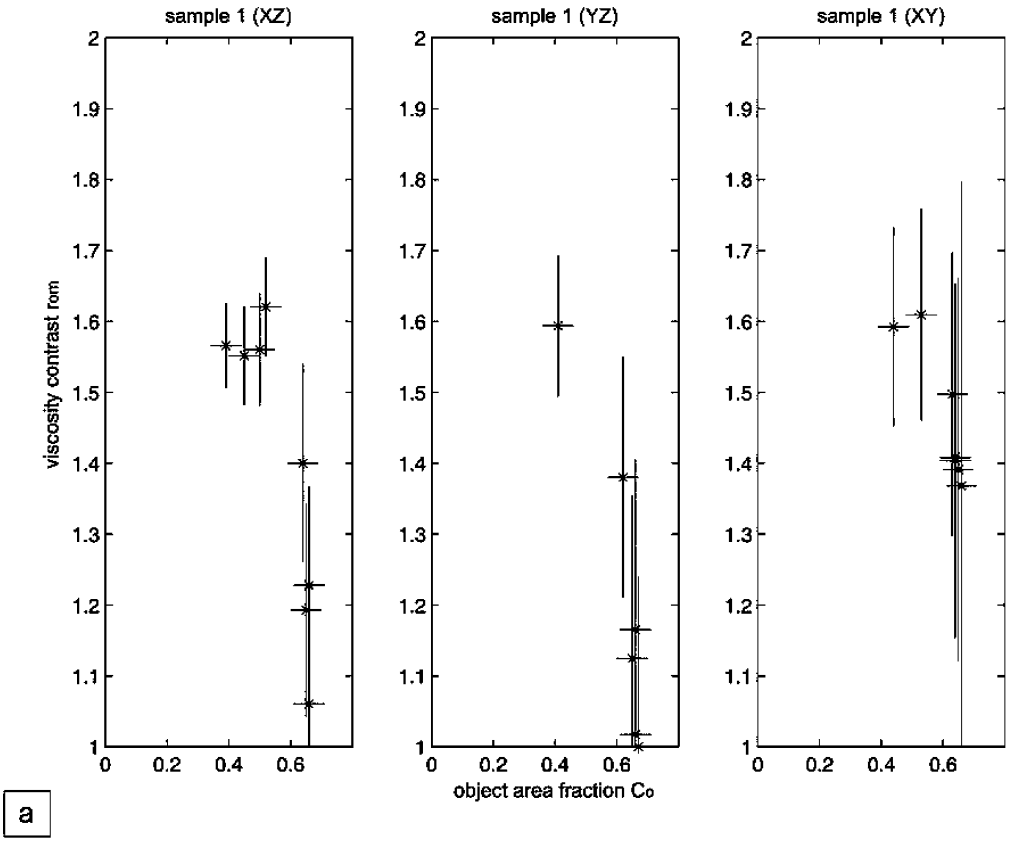

Fig. 5. Plots of viscosity contrast versus object area fraction. (a) Sample 1 (*XZ*, *YZ* and *XY* sections). (b) Samples 2–4 (*XZ* principal sections).

Furthermore, from the r_{om} versus C_o diagrams (Fig. 5) it may be observed that the viscosity contrast reaches the minimum value close to maximum packing, and this value is near to one (representing bulk strain corresponding to object strain), whereas it reaches higher values for lower values of packing.

4.1. Object concentration versus finite strain

Before analysing the interactions between finite strain and object concentration, it is useful to consider the relationships among the three principal sections of the finite strain ellipsoid. The three finite strain values are related by the classical equation (Ramsay, 1967):

$$R_{xy}R_{yz} = R_{xz}. \quad (5)$$

However, it should be noted that Eq. (5) holds where the viscosity contrast is equal to unit—and hence all rock components show the same rheological behaviour. In the case of a system made of two components with different rheological behaviour, the three couples $(R_s,R_o)_{xy,yz,xz}$ must lie on the same curve defined by Eq. (1), as it results from the analysis of naturally deformed rocks (Vitale and Iannace, 2004). As a consequence, Eq. (5) does not hold for systems such as those analysed in this study.

In order to find an empirical law linking finite strain (for objects and rock) and object concentration, we tried curves that, in addition to approximating the (R_o,C_o) and (R_s,C_o) distributions, also satisfy the following conditions (according to the observations by Gay (1968a) and Mandal et al. (2003)): (i) for low values of packing finite strain reaches the maximum value, and it changes slowly with respect to object concentration; and (ii) for high values of packing the curve changes rapidly, and object strain and bulk strain show similar values, converging at R_{min} (Fig. 6).

The best-fit curve we found that satisfies these conditions is:

$$R(C_o) = (R_{max} - R_{min})\left(\frac{(C_o)_{max} - C_o}{(C_o)_{max} + C_o}\right)^{C_o/2} + R_{min}; \quad (6)$$

where R can be either R_o or R_s.

In order to find the values of the parameters included in Eq. (6), we used the MATLAB® curve fitting tool. The best fitting provides the value of R_{max} as the intercept with the ordinate axis, together with the error associated with it (Fig. 6). $(R_s)_{max}$ represents therefore the theoretical bulk finite strain that would be measured in the case of no particle interaction and homogeneous strain at the scale of the sample. This parameter may be considered as a large-scale measure of finite strain, i.e. that corresponding to the distortion of a big circle inscribed in the samples. As the finite strain (R_s) measured by the Fry method is also a function of inclusion concentration, this value does not represent the true bulk strain of the samples; therefore, it may be better termed *effective bulk strain*. On the other hand, being $(R_s)_{max}$ a measure of the bulk deformation experienced by each rock sample as a whole, in the following we shall use the term *real bulk strain* to refer to this value. Similarly, we shall use the terms *effective object strain* (as it is also a function of object concentration) for the finite strain (R_o) obtained by Rf/ϕ analysis and *real object strain* for the calculated maximum value $(R_o)_{max}$.

4.2. Object concentration versus viscosity contrast

In order to find an empirical law that approximates the point distributions in Fig. 4a and b, we can substitute Eq. (6) into Eq. (3):

$$r_{om} = \frac{R_o(C_o)+1}{R_o(C_o)-1}\ln\left(\frac{R_s(C_o)}{R_o(C_o)}\right); \quad (7)$$

Fig. 7a and b shows the related curves. It may be observed that the maximum value of the viscosity contrast $(r_{om})_{max}$ is reached when the object area fraction is equal to zero. We can calculate $(r_{om})_{max}$ putting $(R_o)_{max}$ and $(R_s)_{max}$ into Eq. (3), and $\Delta(r_{om})_{max}$ from Eq. (4). It may also be observed that the minimum value, which is unity, is reached when packing is maximal.

Table 2 shows the values of $(R_o)_{max}$, $\Delta(R_o)_{max}$, $(R_s)_{max}$, $\Delta(R_s)_{max}$, $(r_{om})_{max}$ and $\Delta(r_{om})_{max}$ for sample 1 (full 3D analysis) and for samples 2–4 (2D analysis). The relationships among object concentration, finite strain and viscosity contrast are summarised in Table 3, where $(r_{om})_{effective}$ is the value of r_{om} for C_o that ranges between zero and the maximum packing value. It is worth noting that a similar behaviour is outlined by the curves in Fig. 5, irrespective of the different values of viscosity contrast characterising each sample (ranging from 1.56 to 3.59).

4.3. Effective versus real finite strain

The measured finite strain for objects and rock diminishes where packing is maximal. Therefore, in order to evaluate the departure of measured (i.e. effective) finite strain from the maximum (i.e. real) one, we plotted the ratios $R_o/(R_o)_{max}$ and $R_s/(R_s)_{max}$ versus $C_o/(C_o)_{max}$ (both expressed as a fraction of 100). It may be observed from Fig. 8a that when packing is very high the effective object and bulk strains are significantly lower with respect to R_{max}. Furthermore, the difference is higher for effective bulk strain than for effective object strain. For example, the minimum value of effective bulk strain, which is reached where packing is maximal, is only 43% of the real strain, whereas the minimum value of effective object strain represents 58% of it. However, for packing values below 0.55 (which corresponds to 80% of the maximum observed packing), effective object and bulk strain reach 70–90% of the real value. Fig. 7 also shows that, for object concentrations below 0.55, the viscosity contrast shows homogeneous values plotting around the real value. This

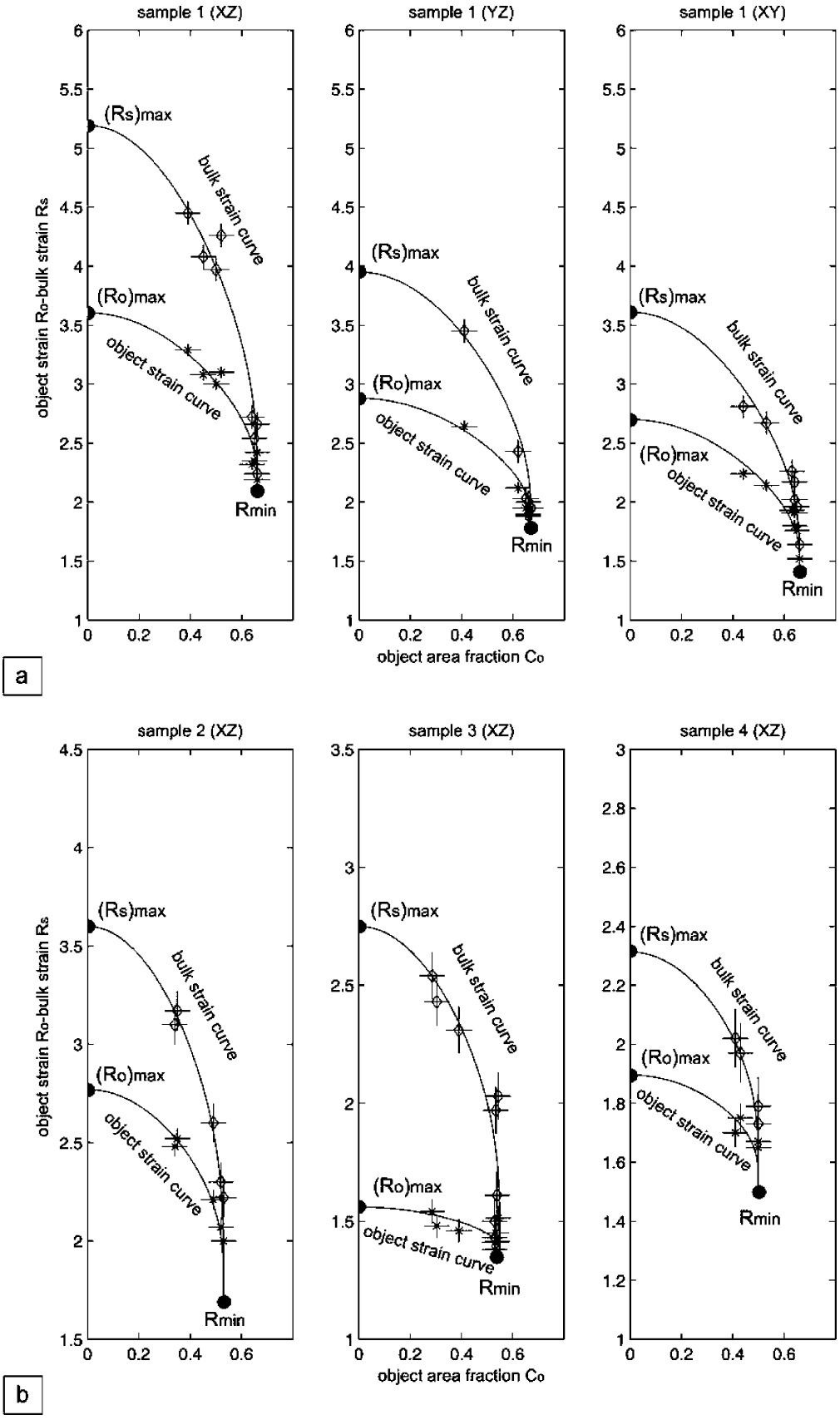

Fig. 6. Plots of Fig. 4a, with curve obtained from empirical Eq. (6) drawn for object and bulk strain. (a) Sample 1 (*XZ*, *YZ* and *XY* principal sections). (b) Samples 2–4 (*XZ* principal sections).

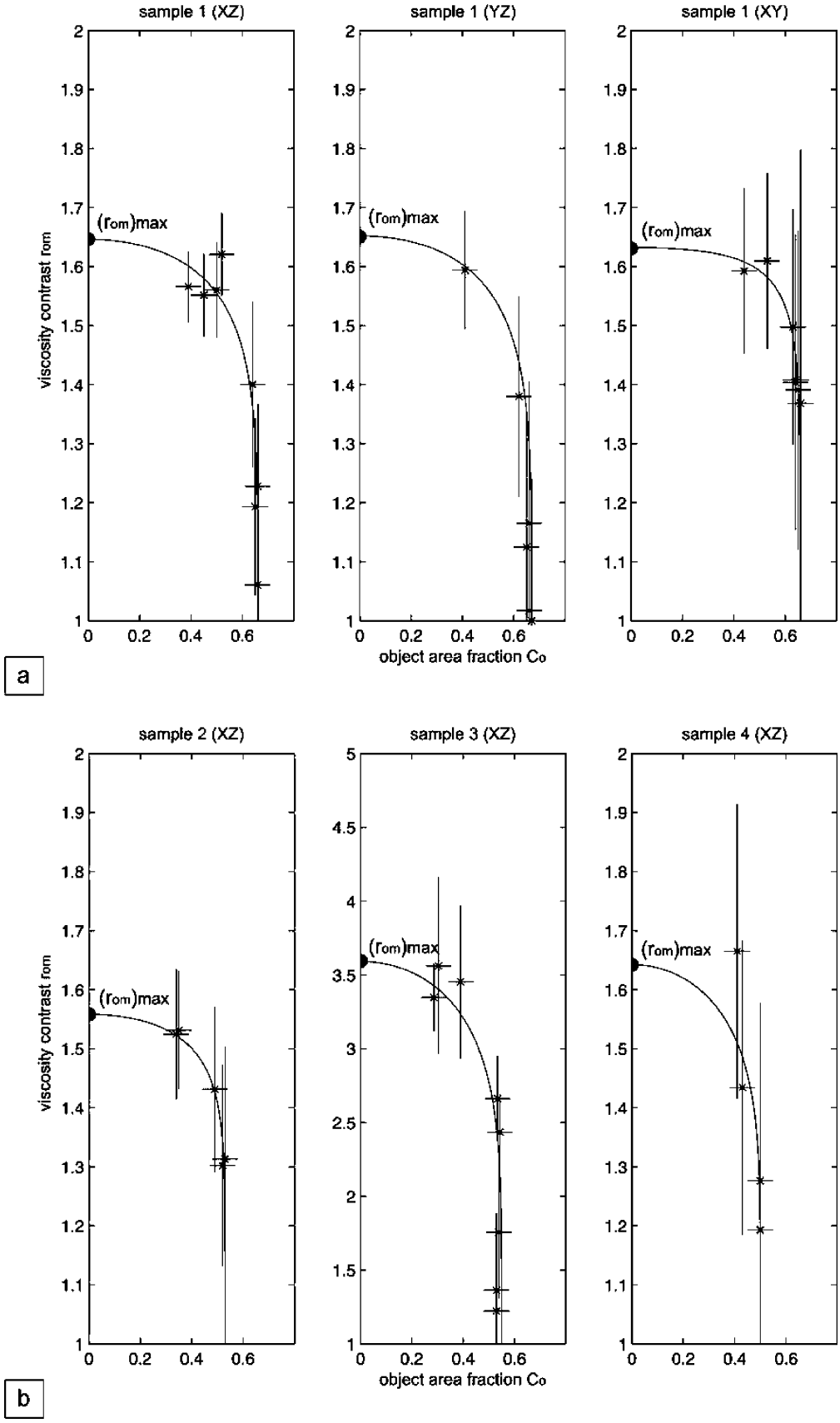

Fig. 7. Plots of Fig. 5, with curve obtained from Eq. (6). (a) Sample 1 (*XZ*, *YZ* and *XY* sections). (b) Samples 2–4 (*XZ* principal sections).

Table 2
Finite strain and viscosity contrast values obtained by best-fit analysis (see text) and Eq. (3)

Sample	Plane	$(R_o)_{max}$	$\Delta(R_o)_{max}$	$(R_s)_{max}$	$\Delta(R_s)_{max}$	R_{min}	$(r_{om})_{max}$	$\Delta(r_{om})_{max}$
1	*XZ*	3.60	0.15	5.19	0.29	2.10	1.65	0.16
1	*YZ*	2.88	0.16	3.95	0.20	1.85	1.65	0.19
1	*XY*	2.72	0.08	3.61	0.13	1.35	1.61	0.13
2	*XZ*	3.77	0.15	3.60	0.26	1.70	1.56	0.19
3	*XZ*	1.56	0.05	2.75	0.24	1.35	3.6	0.4
4	*XZ*	1.90	0.04	3.31	0.03	1.5	1.64	0.04

occurs also for the other samples (Fig. 8b) for which, under a threshold of 70–80% of maximum packing, the viscosity contrast is close to the real value.

4.4. Effective object strain versus effective bulk strain

The behaviour shown in Figs. 6 and 7 is best summarised by plotting R_o and R_s values (relative to the *XZ*, *YZ* and *XY* principal sections for sample 1, and to *XZ* sections for samples 2–4) in a logarithmic diagram in which r_{om}-curves are drawn for different values of viscosity contrast (after Bilby et al., 1975; Gay, 1976). In the same diagram (Fig. 9a and b), the empirical equation (6) is also shown for objects and rock. The empirical curves start from the line representing a unit viscosity contrast (for high values of packing), approaching the line that represents the maximum value of viscosity contrast (for low values of packing). In order to obtain the real viscosity contrast for sample 1 we calculated the mean of the three values of $(r_{om})_{max}$ evaluated for the *XZ*, *YZ* and *XY* planes of the finite strain ellipsoid.

The (R_o,R_s) distribution is scattered over a large area bounded by the lines characterised by $r_{om}=1$ and $r_{om}=(r_o)_{max}$. It can be observed that, when the influence of packing was not taken into account, strain analysis alone could lead to the erroneous inference of dramatic variations of matrix rheology occurring within each sample.

4.5. Object concentration and finite strain ellipsoid shape

Finally, we can plot Eq. (6) for the couples $((R_o)_{XY}, (R_o)_{YZ})$ and $((R_s)_{XY}, (R_s)_{YZ})$ of sample 1 in a Ramsay (1967) logarithmic strain diagram (Fig. 10). It can be observed that for higher values of packing the finite strain ellipsoids are more oblate than for lower values of packing, the difference being of the order of 15–17%. This suggests that, for an equal amount of bulk finite strain, rocks characterised by a high value of packing (such as clast-supported conglomerates) may show a more oblate finite strain ellipsoid with respect to matrix-supported rocks.

5. Conclusions

Our study of naturally deformed, two-component rocks was carried out on limestone samples characterised by variable packing at the scale of the hand specimen, providing the opportunity to quantitatively assess the role of object concentration on finite strain development in rocks otherwise having a constant viscosity contrast. The main conclusions arising from this study are summarised below:

1. Object concentration appears to exert a strong control on strain heterogeneity and finite strain distribution at the scale of the sample.
2. 'Whole-rock' rock strain obtained by applying the Fry analysis is also a function of particle concentration. Therefore, the finite strain (R_s) measured by the Fry method does not represent the true bulk strain of the sample, and is better termed effective bulk strain. On the other hand, an estimate of the real bulk strain of the rock may be obtained by a best-fit curve (Eq. (6)) as the calculated maximum finite strain value $(R_s)_{max}$ (i.e. that expected for homogeneous deformation characterised by no particle interaction).
3. For high values of packing, effective object and bulk strains show values that are significantly lower with respect to the real ones, the difference being 40–60% of the latter.
4. For high values of packing, evaluation of the effective viscosity contrast between objects and matrix furnishes substantially lower values with respect to theoretical maximum ones, and as packing is close to the maximum value, the viscosity contrast approaches a unit value.
5. For low values of packing, the effective viscosity contrast approaches the true value and is equal for the three principal sections of the finite strain ellipsoid.

Table 3
Relationships among object concentration, finite strain and viscosity contrast

Object concentration	Object strain	Bulk strain	Viscosity contrast
$C_o=(C_o)_{max}$	$R_o=R_s=R_{min}$		1
$0<C_o<(C_o)_{max}$	$(R_o)_{max}<R_o<R_{min}$	$(R_s)_{max}<R_s<R_{min}$	$1<(r_{om})_{effective}<(r_{om})_{max}$
$C_o=0$	$(R_o)_{max}$	$(R_s)_{max}$	$(r_{om})_{max}$

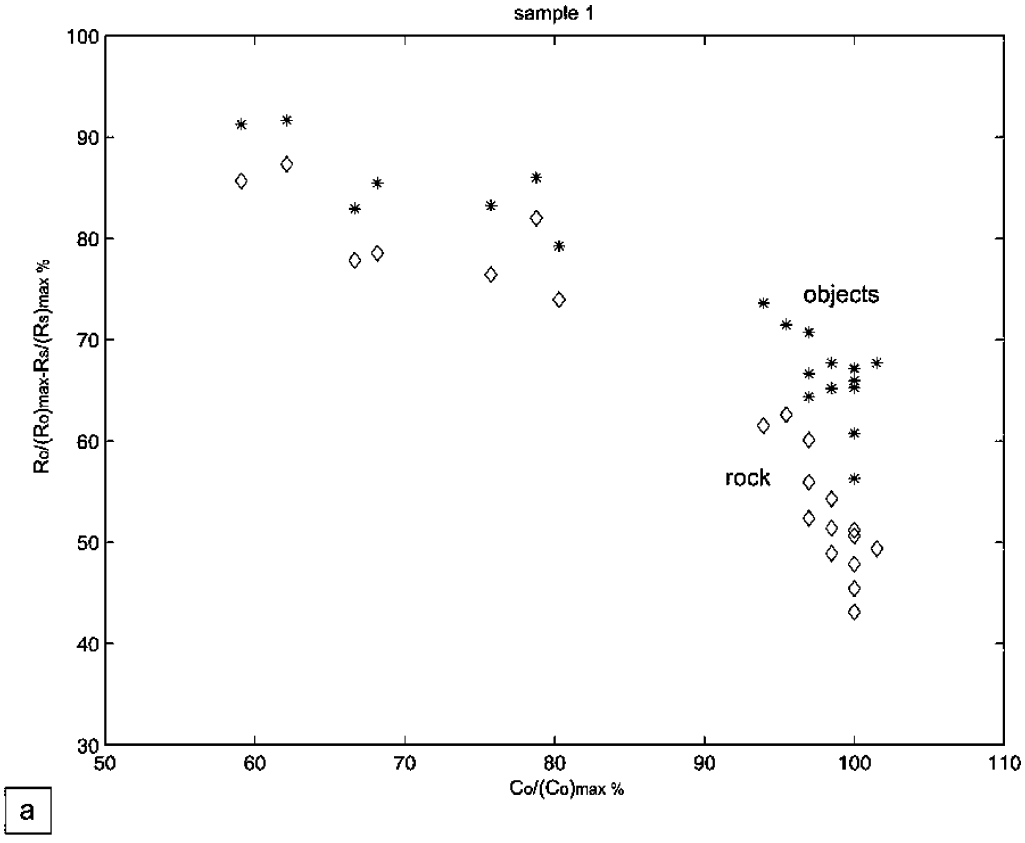

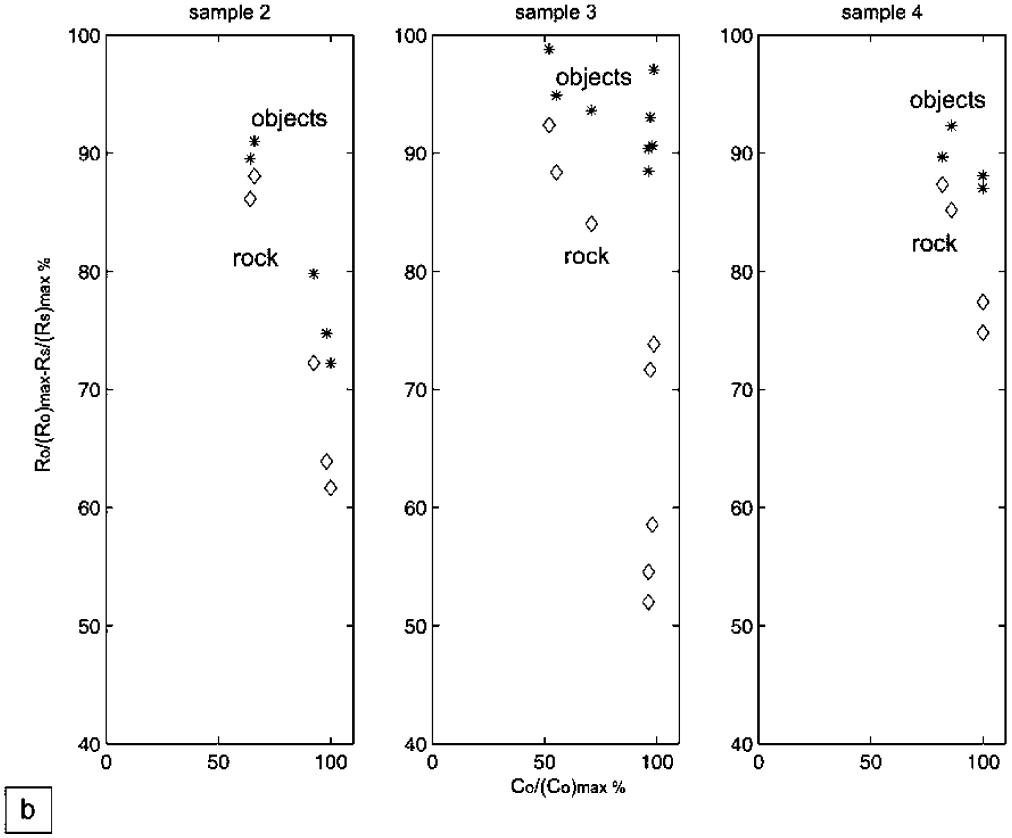

Fig. 8. Plots of $R_o/(R_o)_{max}$ and $R_s/(R_s)_{max}$ versus $C_o/(C_o)_{max}$ (both expressed as a fraction of 100). (a) Sample 1 (*XZ*, *YZ* and *XY* sections). (b) Samples 2–4 (*XZ* principal sections).

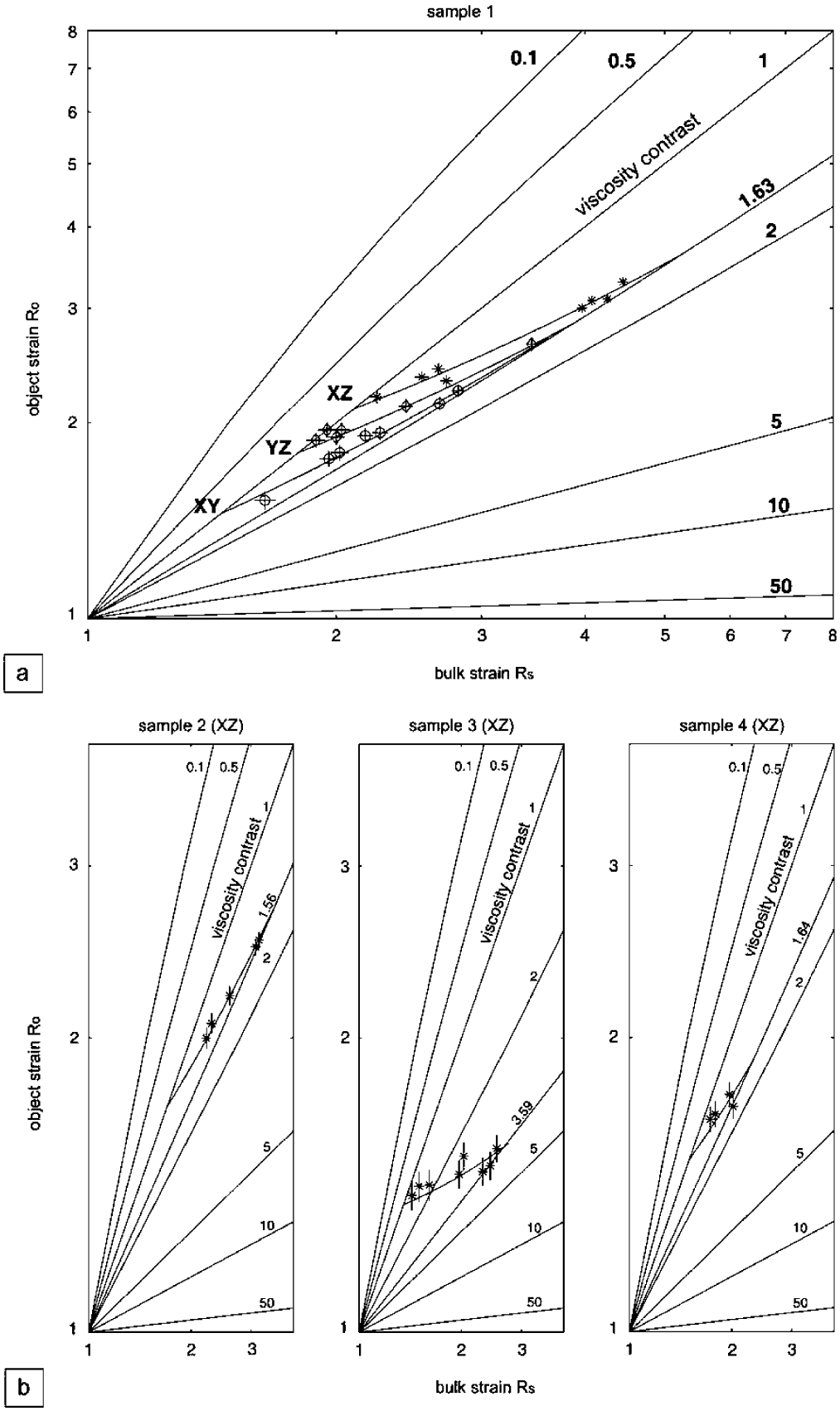

Fig. 9. Plots of effective object strain (R_o) versus effective bulk strain (R_s). (a) Sample 1; diamonds represent $((R_o)_{xz}, (R_s)_{xz})$ couples, stars represent $((R_o)_{yz}, (R_s)_{yz})$ couples and asterisks represent $((R_o)_{xy}, (R_s)_{xy})$ couples. (b) Samples 2–4 (*XZ* principal sections).

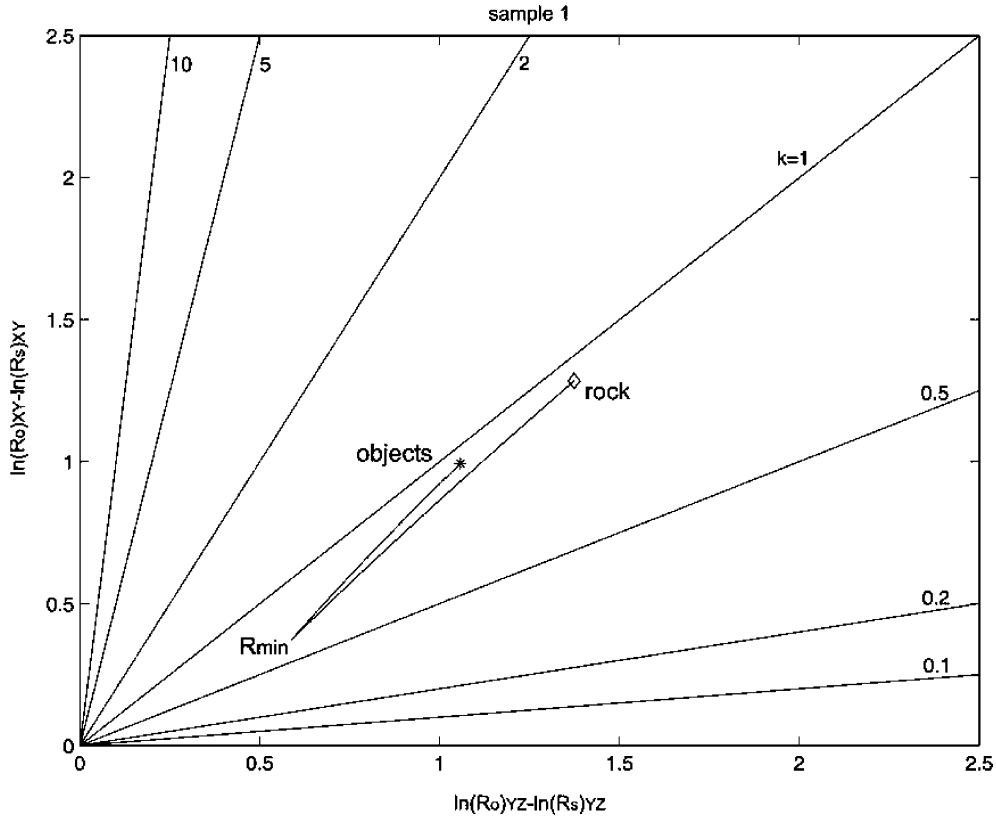

Fig. 10. Curves obtained from empirical Eq. (6) for sample 1, plotted on Ramsay's (1967) logarithmic strain diagram.

6. For high values of packing, object and bulk finite strain ellipsoids are more oblate than for low values of packing.
7. Below a threshold of 70–80% of the maximum packing, effective object and bulk finite strains reach a value that is close to the real one. Furthermore, the calculated viscosity contrast is also close to the real value, being within the range of statistical error of the measured effective viscosity contrast.
8. Empirical equations may be obtained, describing the relationships between object concentration and the parameters of object strain, bulk strain and viscosity contrast.

Our results provide a quantitative assessment of some of the problems inherent to finite strain analysis in rocks consisting of objects and matrix. The implemented empirical equations may also allow structural geologists to handle finite strain and viscosity contrast data obtained from such rocks with more accuracy and to obtain valuable paleorheological information.

Acknowledgements

The paper greatly benefited from discussions with Joe White, Neil Mancktelow and several people at the DRT Conference in Zurich (May 2005). Thorough and constructive reviews by Richard Lisle and an anonymous referee helped to improve the paper.

References

Bilby, B.A., Eshelby, J.D., Kundu, A.K., 1975. The change of shape of a viscous ellipsoidal region embedded in a slowly deforming matrix having a different viscosity. Tectonophysics 28, 265–274.

Cloos, E., 1947. Oolite deformation in south mountain fold, Maryland. Geological Society of America Bulletin 58, 843–918.

Dunnet, D., 1969. A technique of finite strain analysis using elliptical particles. Tectonophysics 7, 117–136.

Erslev, E.A., 1988. Normalized center-to-center strain analysis of packed aggregates. Journal of Structural Geology 10, 201–209.

Fry, N., 1979. Random point distributions and strain measurement in rocks. Tectonophysics 60, 89–105.

Gay, N.C., 1968a. Pure shear and simple shear deformation of inhomogeneous viscous fluids. 1. Theory. Tectonophysics 5, 211–234.

Gay, N.C., 1968b. Pure shear and simple shear deformation of inhomogeneous viscous fluids. 2. The determination of the total finite strain in a rock from inclusions such as deformed pebbles. Tectonophysics 5, 295–302.

Gay, N.C., 1976. The change of shape of a viscous ellipsoidal region embedded in a slowly deforming matrix having a different viscosity—a discussion. Tectonophysics 35, 403–407.

Iannace, A., Vitale, S., 2004. Ductile shear zones on carbonates: the Calcaires plaquettés of northern Calabria (Italy). Comptes Rendus Geoscience 336, 227–234.

Lisle, R.J., 1979. Strain analysis using deformed pebbles: the influence the initial pebble shape. Tectonophysics 60, 263–277.

Lisle, R.J., 1985. Geological Strain Analysis. A Manual for the Rf/ϕ Technique. Pergamon Press, Oxford.

Lisle, R.J., Rondeel, H.E., Doorn, D., Brugge, J., van de Gaag, P., 1983. Estimation of viscosity contrast and finite strain from deformed elliptical inclusions. Journal of Structural Geology 5, 603–609.

Mandal, N., Samanta, S.K., Bhattacharyya, G., Chakraborty, C., 2003. Deformation of ductile inclusions in a multiple inclusion system in pure shear. Journal of Structural Geology 25, 1359–1370.

Ramsay, J.G., 1967. Folding and Fracturing of Rocks. McGraw-Hill, New York.

Ramsay, J.G., Huber, M., 1983. Strain Analysis, The Techniques of Modern Structural Geology, vol. I. Academic Press, London.

Treagus, S.H., Treagus, J.E., 2001. Effects of object ellipticity on strain, and implications for clast-matrix rocks. Journal of Structural Geology 23, 601–608.

Treagus, S.H., Treagus, J.E., 2002. Studies of strain and rheology of conglomerates. Journal of Structural Geology 24, 1541–1567.

Vitale, S., Iannace, A., 2004. Analisi dello strain finito in 3D dell'Unità Pollino-Ciagola (confine calabro-lucano, Italia meridionale). Studi Geologici Camerti Nuova Serie 2, 153–167.